1-1-2016

Non-smooth feedback control for Belousov-Zhabotinskii reaction-diffusion equations: semi-analytical solutions

Hassan Alfifi
The University of Dammam, hyja973@uowmail.edu.au

Timothy R. Marchant
University of Wollongong, tim@uow.edu.au

Mark Nelson
University of Wollongong, mnelson@uow.edu.au

Non-smooth feedback control for Belousov-Zhabotinskii reaction-diffusion equations: semi-analytical solutions

Abstract

The Belousov-Zhabotinskii reaction is considered in one and two-dimensional reaction-diffusion cells. Feedback control is examined where the feedback mechanism involves varying the concentrations in the boundary reservoir, in response to the concentrations in the centre of the cell. Semi-analytical solutions are developed, via the Galerkin method, which assumes a spatial structure for the solution, and is used to approximate the governing delay partial differential equations by a system of delay ordinary differential equations. The form of feedback control considered, whilst physically realistic, is non-smooth as it has discontinuous derivatives. A stability analysis of the sets of smooth delay ordinary differential equations, which make up the full non-smooth system, allows a band of Hopf bifurcation parameter space to be obtained. It is found that Hopf bifurcations for the full non-smooth system fall within this band of parameter space. In the case of feedback with no delay a precise semi-analytical estimate for the stability of the full non-smooth system can be obtained, which corresponds well with numerical estimates. Examples of limit cycles and the transient evolution of solutions are also considered in detail.

Disciplines

Engineering | Science and Technology Studies

Publication Details

Alfifi, H. Y., Marchant, T. R. & Nelson, M. I. (2016). Non-smooth feedback control for Belousov-Zhabotinskii reaction-diffusion equations: semi-analytical solutions. Journal of Mathematical Chemistry, 54 (8), 1632-1657.

Non-smooth feedback control for Belousov-Zhabotinskii reaction-diffusion equations: semi-analytical solutions

H.Y. Alfifi · T. R. Marchant · M. I. Nelson

August 25, 2016

Abstract The Belousov-Zhabotinskii reaction is considered in one and two-dimensional reaction-diffusion cells. Feedback control is examined where the feedback mechanism involves varying the concentrations in the boundary reservoir, in response to the concentrations in the centre of the cell. Semi-analytical solutions are developed, via the Galerkin method, which assumes a spatial structure for the solution, and is used to approximate the governing delay partial differential equations by a system of delay ordinary differential equations. The form of feedback control considered, whilst physically realistic, is non-smooth as it has discontinuous derivatives. A stability analysis of the sets of smooth delay ordinary differential equations, which make up the full non-smooth system, allows a band of Hopf bifurcation parameter space to be obtained. It is found that Hopf bifurcations for the full non-smooth system fall within this band of parameter space. In the case of feedback with no delay a precise semi-analytical estimate for the stability of the full non-smooth system can be obtained, which corresponds well with numerical estimates. Examples of limit cycles and the transient evolution of solutions are also considered in detail.

Keywords mathematical modelling, reaction-diffusion-delay equations, Belousov-Zhabotinskii, Hopf bifurcations, non-smooth feedback control

Mathematics Subject Classification (2000) 35,37,41

1 Introduction

Oscillatory phenomena in chemical systems have been studied, by both theoreticians and experimentalists, for many decades. The Belousov-Zhabotinskii (BZ) reaction, Bray-Liebhafsky and Briggs-Rauscher systems undergo periodic concentration variations and have the added interest that these oscillations can be visualized via colour changes, see [1]. The BZ reaction, discovered by Belousov [2] in 1951, is a classical one used for understanding periodic chemical and biological relaxation oscillations. The BZ reaction has a rich history of experimental, theoretical and numerical study. The range of phenomena for which the BZ reaction, and other chemical oscillator systems, prove a useful test-bed include multi-stability, chaos, bursting, reaction-diffusion patterns and waves and feedback control, see Sagues and Epstein [3] for a comprehensive review of these phenomena in the context of chemical systems.

H.Y. Alfifi
School of Mathematics and Statistics, The University of Dammam, Dammam, Eastern, 31441, Saudi Arabia

T. R. Marchant · M. I. Nelson
School of Mathematics and Applied Statistics, The University of Wollongong, Wollongong, 2522, N.S.W., Australia.
E-mail: tim_marchant@uow.edu.au

Field et al. [4] described the chemistry of the BZ reaction and presented experimental data illustrating the sustained oscillations, rate constants for the reactions and stated the ten component reactions fundamental to the system. There have been many subsequent approaches used to simplify the original system of BZ equations. Field and Noyes [5] developed the Oregonator model, which consists of three coupled ODEs, to model the five most important BZ reactions, while [6,7] proposed the Oregonator model

$$\epsilon\frac{du}{dt} = qv - uv + u(1-u), \quad \delta\frac{dv}{dt} = -qv - uv + fw, \quad \frac{dw}{dt} = u - w, \tag{1}$$
$$\text{where } \epsilon = 4\times10^{-2}, \delta = 2\times10^{-4}, q = 8\times10^{-4},$$

where u, v and w are the reactant concentrations.

Marchant [8] considered the Gray & Scott cubic autocatalytic model in a reaction-diffusion cell. The Galerkin method was used to obtain a lower-order ODE model, as an approximation to the governing PDE system. Singularity and bifurcation theory theory was then used to obtain semi-analytical steady-state solutions and bifurcation diagrams, together with the region of parameter space, where Hopf bifurcations occur. The comparison between the semi-analytical and numerical solutions of the governing PDEs was found to be excellent. Marchant [9] extended these ideas to the Gray–Scott model with Michaelis–Menten decay. The Fourier Galerkin series solution method has also been used to obtain numerical solutions to a steady-state diffusive BZ equation by Forbes [10, 11]. He found a stripy pattern, corresponding to a standing wave and that the spatial pattern is not necessarily unique. It was also shown that small amplitude patterns are not stable but that large-amplitude patterns may be quasi-stable.

Experimental studies of spatial phenomena for oscillatory chemical systems have relied on the development of new types of reactors, which allow the influx of fresh reactants without stirring the reactor contents. This has been achieved by the use of gel filled reactors (which prevents advective motion) coupled to well-stirred reactant reservoirs at the boundaries. Early experiments with gel reactors were performed by Noszticzius et al. [12] and Tam et al. [13] who reported results for the BZ reaction while later studies by Bagyan et al. [14] and Lavrova et al. [15] considered glycolytic reactions.

Feedback control can be applied to chemical systems to achieve the stabilization of limit cycles and unstable steady states and also to generate chaotic behaviour. Sriram [16] studied numerical and experimental simulations of electrical feedback for the BZ reaction in a CSTR reactor. The amplitude and period of the limit cycle oscillations were increased by the feedback and it was shown that the experimental observations were accurately modelled by the Oregonator model, with a feedback term added to one of the dynamic variables. Bifurcation diagrams were drawn and the effect of positive feedback on the Hopf bifurcation parameter region was investigated numerically. Vanag et al. [17] performed numerical simulations of the BZ reaction. They used a three-variable model of the BZ reaction, proposed by [18], and obtained good comparisons between their simulations and experimental data. The control parameter was the inflow rate for the CSTR. They showed that there are two simple ways to modify the transition from chaotic behaviour, by varying the strength of the feedback and the delay response. Lipták et al. [19] considered a general open CSTR system obeying the mass action law. They proposed a class of polynomial feedback that stabilizes the system, which can then be described by a generalized Hamiltonian form. Vanag and Epstein [20] reviewed the design and control of patterns in both batch oscillators and gel reactors. Some of the varied control methods discussed include the use of initial conditions, photochemical control, periodic forcing and temperature.

di Bernardo et al. [21] considered bifurcation theory for non-smooth piecewise continuous ODE systems. Many important applications, such as control and switching problems, impact oscillators and friction systems, are governed by such systems. They reviewed bifurcation theory for steady-state solutions, which lie on discontinuity boundaries, and described the new types of instabilities which can occur in the non-smooth system. Camlibel et al. [22] considered the stability of a plane piecewise smooth linear system with two dependent variables and discontinuous derivatives at the steady-state solution. They derived the conditions for the overall stability of the non-smooth system, which relate the complex eigenvalues of the two smooth systems. Csikja et al. [23]

considered a linear piecewise affine ODE model of hysteresis. They constructed piecewise smooth limit cycle solutions and considered their stability.

In this paper, we study the Oregonator model (1) in a reaction-diffusion cell with feedback control. The feedback consists of varying the concentrations in the boundary reservoirs in response to the concentrations in the centre of the cell. A delay in the response time is also modelled. Also, to be physically realistic, the concentrations at the boundary must be positive, which requires the introduction of a modulus term in the feedback response, leading to a non-smooth system. This study has a number of aims; to illustrate that the Galerkin averaging method is useful in accurately approximating the full reaction-diffusion BZ system, to explore the effect of feedback on the BZ system, and to illustrate how approximations can be found that predict Hopf bifurcations for non-smooth systems. Moreover the Oregonator model represents a classical prototype for analyzing chemical oscillations; analytical techniques found to be useful here can potentially be applied to the vast range of other chemical oscillators known to exist (see, for example, figure 3 of Sagues and Epstein [3]) for which the number of chemical species is very large and the corresponding sets of model equations do not enjoy the simplicity of the classical Oregonator.

In Section 2 the semi-analytical model, consisting of a set of non-smooth delay ODEs, is derived by using the Galerkin method. In Section 3 steady-state solutions are found. In Section 4 the prediction of regions of parameters space, in which Hopf bifurcations occur, is considered in detail. The non-smooth system consist of eight different sets of smooth delay ODEs. The stability of each smooth ODE system is found and combined. This approach gives three regions, a region in which all smooth parts of the system are stable, a region in which all are unstable, and an intermediate region where some smooth systems are stable and some are unstable. Hopf bifurcations for the full non-smooth system always occur in this intermediate band of parameter space. In the case of no delay a precise prediction of the Hopf bifurcation parameter space, of the full non-smooth system, is found by considering the dominant eigenvalues and the ideas of [21,22]. A good comparison between the semi-analytical model and numerical results is also obtained, for steady-state solutions, the transient evolution to the steady-state and for limit cycles.

2 The semi-analytical model

2.1 Model equations

The BZ equations in a 2-D reaction-diffusion cell have the form

$$\frac{du}{dt} = k\nabla^2 u + \frac{1}{\epsilon}\left(qv - uv + u(1-u)\right), \quad \frac{dv}{dt} = k\nabla^2 v + \frac{1}{\delta}\left(fw - qv - uv\right), \tag{2}$$

$$\frac{dw}{dt} = k\nabla^2 w + u - w,$$

$$u = v = w = 0 \ \text{ at } x, y = \pm 1, \quad u = u_a, \quad v = v_a, \quad w = w_a, \quad t = 0, \tag{3}$$

The system (2) is the BZ model proposed by [6], with Dirichlet boundary conditions (3). In 1-D we consider the natural simplification of (2) where the concentrations in the y-direction are uniform. The equations are in non-dimensional form with the scaled reactant concentrations, u, v and w. It is an open system; the reactor has a permeable boundary at $x, y = \pm 1$, joined to a reservoir in which the reactants have zero concentrations, see [12,13] for experimental scenarios. The parameters $k, f, \epsilon, \delta, q$, defined in (1), are all positive where f is termed the stoichiometric factor and k the diffusion coefficient. Jahnke and Winfree [26] report that the range $f \in [0, 4]$ for chemical systems. We let (u_s, v_s, w_s) be the steady-state concentrations at the centre of the reactor $x = y = 0$. The initial concentrations are (u_a, v_a, w_a).

We are interested in examining the effect of feedback on the reaction-diffusion cell (2) so consider the following feedback algorithm

$$u = H|u_s - u(0,0,t-\tau)|, \ v = H|v_s - v(0,0,t-\tau)| \tag{4}$$

$$w = H|w_s - w(0,0,t-\tau)|, \quad \text{at } x, y = \pm 1,$$

where the reservoir concentrations are altered, in response to the concentrations in the cell at the centre of the cell (located at $x = y = 0$). Many studies have been undertaken of feedback control for CSTRs, where the flow rate is altered in response to the concentrations in the reactor; (4) represents an analogous form of feedback control for a reaction-diffusion cell, see [3,24,25].

Experimentally this can be achieved using a diffusive gel coupled to a CSTR, which represents the reservoir; [13] considered a BZ reaction while [14,15] considered a glycolytic reaction. The inert gel medium prevents convective motion but allows diffusion of the chemical species. By using high flow rates the concentrations in the CSTR remain close to the input values and the chemical reactions in the CSTR can be neglected.

The feedback is proportional to the difference between the transient concentrations and the steady-state values at the centre of the cell, while H is the strength of the feedback and τ is the delay response. The feedback response is zero at the steady-state so (4) does not alter the steady-state solutions of (2) and we investigate the effect of this feedback control on the stability of the reaction-diffusion cell. Note that the concentrations must always be positive in the reservoir, hence the modulus signs on the feedback terms. The modulus terms result in a continuous feedback system but with non-smooth derivatives.

A Crank–Nicolson finite-difference scheme is used to find the numerical solutions of the governing PDE system. This implicit scheme is unconditionally stable. A fourth-order Runge–Kutta scheme is used to solve the semi-analytical ODE models. Other numerical methods, such as operator splitting, exist for this class of reaction diffusions equations, see for example, Ropp and Shadid [27].

2.2 The Galerkin method

The semi-analytical models for (2) in the 1-D and 2-D geometries are found using a Galerkin method. This method assumes a spatial structure of the concentration profiles, see [28,8]. The Galerkin method allows the governing delay PDE to be approximated by a system of delay ODEs. In 1-D we use the expansion

$$\begin{aligned}
u(x,t) &= (u_1(t) - H|u_{1s} + u_{2s} - u_{1d} - u_{2d}|)\cos\left(\frac{\pi}{2}x\right) \\
&\quad + u_2(t)\cos\left(\frac{3\pi}{2}x\right) + H|u_{1s} + u_{2s} - u_{1d} - u_{2d}|, \\
v(x,t) &= (v_1(t) - H|v_{1s} + v_{2s} - v_{1d} - v_{2d}|)\cos\left(\frac{\pi}{2}x\right) \\
&\quad + v_2(t)\cos\left(\frac{3\pi}{2}x\right) + H|v_{1s} + v_{2s} - v_{1d} - v_{2d}|, \\
w(x,t) &= (w_1(t) - H|w_{1s} + w_{2s} - w_{1d} - w_{2d}|)\cos\left(\frac{\pi}{2}x\right) \\
&\quad + w_2(t)\cos\left(\frac{3\pi}{2}x\right) + H|w_{1s} + w_{2s} - w_{1d} - w_{2d}|.
\end{aligned} \tag{5}$$

The subscript d implies a delay, that is $u_{1d} = u_1(t-\tau)$. The trial functions are chosen so that $u_1 + u_2$, $v_1 + v_2$ and $w_1 + w_2$ are the concentrations at the centre of the reaction-diffusion cell and so the boundary conditions at $x = \pm 1$ are satisfied. Note that the form of (5) is not unique; a more symmetric form for could be chosen or quadratic expressions for the spatial profiles could be used, but the level of accuracy of the method is usually independent of the forms of the basis functions used. The PDEs (2) are not satisfied exactly, but the free parameters in this expansion are obtained by evaluating averaged versions of the governing equations, weighted by the basis functions $\cos\left(\frac{1}{2}\pi x\right)$ and $\cos\left(\frac{3}{2}\pi \mathrm{x}\right)$. Then, the ODEs

$$\frac{du_1}{dt} = \frac{\pi}{H\pi - 4H + \pi}\left[-\frac{k\pi^2}{4}u_1 - \frac{1}{\epsilon\pi}\left(\frac{8}{15}u_2v_1 + \frac{16}{15}u_1u_2 + \frac{72}{35}u_2v_2\right)\right.$$

$$
\begin{aligned}
&- \frac{1}{\epsilon\pi}\left(\frac{8}{15}u_1v_2+\frac{72}{35}u_2^2+\frac{8}{3}u_1^2+\frac{8}{3}u_1v_1-\pi q v_1-\pi u_1\right)+HM_1\Big],\\
\frac{dv_1}{dt} &= \frac{\pi}{H\pi-4H+\pi}\Big[-\frac{k\pi^2}{4}v_1-\frac{1}{\delta\pi}\left(\frac{8}{3}u_1v_1+\frac{8}{15}u_1v_2+\frac{72}{35}u_2v_2\right)\\
&- \frac{8}{15\delta\pi}u_2v_1+\frac{1}{\delta}fw_1-\frac{1}{\delta}qv_1+HM_2\Big],\\
\frac{dw_1}{dt} &= \frac{\pi}{H\pi-4H+\pi}\Big[-\frac{k\pi^2}{4}w_1+u_1-w_1+HM_3\Big],\\
\frac{du_2}{dt} &= \frac{3\pi}{4H+3\pi}\Big[-\frac{9k\pi^2}{4}u_2-\frac{1}{\epsilon\pi}\left(\frac{8}{15}u_1^2-\frac{8}{9}u_2^2+\frac{8}{15}u_1v_1+\frac{72}{35}u_1v_2\right)\\
&+ \frac{1}{\epsilon\pi}\left(\frac{8}{9}u_2v_2-\frac{72}{35}u_2v_1-\frac{144}{35}u_1u_2+\pi q v_2+\pi u_2\right)+HM_4\Big],\\
\frac{dv_2}{dt} &= \frac{3\pi}{4H+3\pi}\Big[-\frac{9k\pi^2}{4}v_2-\frac{1}{\delta\pi}\left(\frac{8}{15}u_1v_1+\frac{72}{35}u_1v_2+\frac{72}{35}u_2v_1\right)\\
&+ \frac{8}{9\delta\pi}u_2v_2+\frac{1}{\delta}fw_2-\frac{1}{\delta}qv_2+HM_5\Big],\\
\frac{dw_2}{dt} &= \frac{3\pi}{4H+3\pi}\Big[-\frac{9k\pi^2}{4}w_2+u_2-w_2+HM_6\Big],
\end{aligned}
\tag{6}
$$

are obtained, where the M_i are given in the Appendix. The series in (5) has been truncated after two terms. The number of terms that are used in the truncated series represents a trade-off between the accuracy and complexity of the semi-analytical solution. It is found that a two-term method gives sufficient accuracy without excessive expression swell. A one-term solution is found by letting each of u_2, v_2 and w_2 equal to zero. As the M_i includes modulus terms, the ODEs (6) represent a non-smooth system (as there are discontinuous derivatives). Moreover, as there are three different modulus terms the non-smooth system (6) is composed of eight different smooth ODE systems.

For the 2-D geometry, the expansion

$$
\begin{aligned}
u(x,y,t) &= (u_1(t)-H|u_{1s}+u_{2s}-u_{1d}-u_{2d}|)\cos\left(\frac{1}{2}\pi x\right)\cos\left(\frac{1}{2}\pi y\right)\\
&+ u_2(t)\cos\left(\frac{3}{2}\pi x\right)\cos\left(\frac{1}{2}\pi y\right)+u_2(t)\cos\left(\frac{1}{2}\pi x\right)\cos\left(\frac{3}{2}\pi y\right)\\
&+ H|u_{1s}+u_{2s}-u_{1d}-u_{2d}|,\\
v(x,y,t) &= (v_1(t)-H|v_{1s}+v_{2s}-v_{1d}-v_{2d}|)\cos\left(\frac{1}{2}\pi x\right)\cos\left(\frac{1}{2}\pi y\right)\\
&+ v_2(t)\cos\left(\frac{3}{2}\pi x\right)\cos\left(\frac{1}{2}\pi y\right)+v_2(t)\cos\left(\frac{1}{2}\pi x\right)\cos\left(\frac{3}{2}\pi y\right)\\
&+ H|v_{1s}+v_{2s}-v_{1d}-v_{2d}|,\\
w(x,y,t) &= (w_1(t)-H|w_{1s}+w_{2s}-w_{1d}-w_{2d}|)\cos\left(\frac{1}{2}\pi x\right)\cos\left(\frac{1}{2}\pi y\right)\\
&+ w_2(t)\cos\left(\frac{3}{2}\pi x\right)\cos\left(\frac{1}{2}\pi y\right)+w_2(t)\cos\left(\frac{1}{2}\pi x\right)\cos\left(\frac{3}{2}\pi y\right)\\
&+ \quad H|w_{1s}+w_{2s}-w_{1d}-w_{2d}|.
\end{aligned}
\tag{7}
$$

is used, which also satisfies the relevant 2-D geometry boundary conditions in (2). Symmetry implies that two of the terms have the same coefficient. Averaging using the weights $\cos\left(\frac{1}{2}\pi x\right)\cos\left(\frac{1}{2}\pi y\right)$ and $\cos\left(\frac{1}{2}\pi x\right)\cos\left(\frac{3}{2}\pi y\right)$, gives the following ODE model

$$
\frac{du_1}{dt} = \frac{\pi^2}{H\pi^2-16H+\pi^2}\Big[-\frac{k\pi^2}{2}u_1-\frac{1}{\epsilon\pi^2}\left(\frac{64}{9}u_1v_1+\frac{128}{45}u_1v_2-\pi^2 q v_1\right)
$$

$$
\begin{aligned}
&- \frac{1}{\epsilon\pi^2}\left(\frac{18176}{1575}u_2v_2 + \frac{128}{45}u_2v_1 + \frac{256}{45}u_1u_2 + \frac{64}{9}u_1^2 - \pi^2u_1\right) + HN_1\Bigg], \\
\frac{dv_1}{dt} &= \frac{\pi^2}{H\pi^2 - 16H + \pi^2}\left[-\frac{k\pi^2}{2}v_1 - \frac{1}{\delta\pi^2}\left(\frac{64}{9}u_1v_1 + \frac{128}{45}u_1v_2 + \pi^2qv_1\right)\right. \\
&- \frac{18176}{1575\delta\pi^2}u_2v_2 - \frac{128}{45\delta\pi^2}u_2v_1 + \frac{1}{\delta}fw_1 + HN_2\Bigg], \\
\frac{dw_1}{dt} &= \frac{\pi^2}{H\pi^2 - 16H + \pi^2}\left[-\frac{k\pi^2}{2}w_1 + u_1 - w_1 + HN_3\right], \\
\frac{du_2}{dt} &= \frac{3\pi^2}{16H + 3\pi^2}\left[-\frac{5k\pi^2}{2}u_2 - \frac{1}{\epsilon\pi^2}\left(\frac{64}{45}u_1v_1 + \frac{9088}{1575}u_1v_2 + \frac{9088}{1575}u_2v_1\right)\right. \\
&- \frac{1}{\epsilon\pi^2}\left(\frac{64}{45}u_1^2 + \frac{18176}{1575}u_1u_2 + \frac{4352}{4725}u_2v_2 + \frac{4352}{4725}u_2^2 - \pi^2u_2\right) \\
&+ \frac{qv_2}{\epsilon} + HN_4\Bigg], \\
\frac{dv_2}{dt} &= \frac{3\pi^2}{16H + 3\pi^2}\left[-\frac{5k\pi^2}{2}v_2 - \frac{1}{\delta\pi^2}\left(\frac{64}{45}u_1v_1 + \frac{4352}{4725}u_2v_2 + \frac{9088}{1575}u_1v_2\right)\right. \\
&- \frac{9088}{1575\delta\pi^2}u_2v_1 - \frac{1}{\delta}qv_2 + \frac{1}{\delta}fw_2 + HN_5\Bigg], \\
\frac{dw_2}{dt} &= \frac{3\pi^2}{16H + 3\pi^2}\left[-\frac{5k\pi^2}{2}w_2 + u_2 - w_2 + HN_6\right].
\end{aligned}
\tag{8}
$$

where N_i are given in the Appendix.

3 Steady-state solutions

In this section we study the steady-state solutions of the semi-analytical model for the 1-D and 2-D geometries. In order to find steady-state solutions, we let $u(t) = u_s, v(t) = v_s$ and $w(t) = w_s$ in the ODE models, which reduces them to sets of transcendental equations. At the steady state, the feedback terms, involving H, are all zero. The steady-state solutions for the 1-D and 2-D geometries are found by solving the transcendental equations using a root-finding routine from the Maple software package. For all figures in this section the diffusion coefficient $k = 1$ and ϵ, δ, q are given in (1).

Figure 1 shows the steady-state reactant concentrations u, v and w versus stoichiometric factor f, for the 1-D geometry. Shown are the one and two-term semi-analytical and numerical solutions at the centre of the domain, $x = 0$. There is a unique steady-state solution for the reactant concentrations. The figures show u and w decrease as f increases, before approaching a minimum at large f. However, the curve for v increases as f increases. Hence, for large f, u and w are near zero while v increases linearly. There is an excellent comparison between the two-term semi-analytical and numerical solutions, with less than 2.5% error for all values of stoichiometric factors up to $f = 10$. The concentration versus f response curve for the non-diffusive BZ system (the classical Oregonator model (1)), is qualitatively similar to figure 1 with a unique steady-state solution (see Field and Noyes [5]).

Figure 2 shows the steady-state reactant concentrations u, v and w versus x, for the 1-D geometry. Shown are the one-term and two-term semi-analytical and numerical solutions of the governing PDE. The stoichiometric factor $f = 8$. The solution for the reactant concentration u has two humps, for the two-term semi-analytical and numerical solutions, while the other reactants have a single central peak. The two-term solution can model the non-central peak accurately while the one-term solution cannot. The comparison between the two-term semi-analytical and numerical solutions is excellent, while the one-term solution is reasonably accurate at the centre of the domain, $x = 0$. These behaviours are qualitatively similar to the concentration profiles in cubic auto-catalytic reactions, see [8].

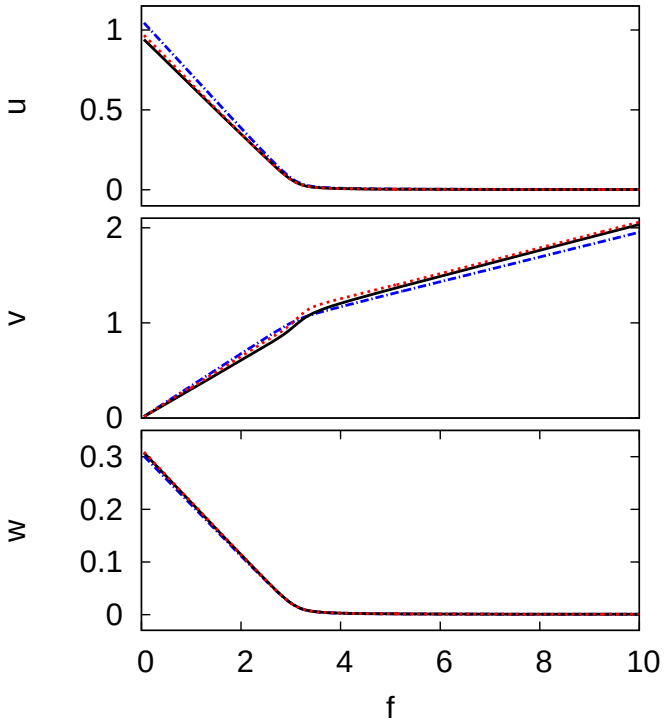

Fig. 1 (color online) The steady-state reactant concentrations u, v and w versus stoichiometric factor f, at $x = 0$, for the 1-D geometry. Shown are the one-term (dashed blue line) and two-term (black solid line) semi-analytical solutions and numerical (red dotted line) solutions of the governing PDEs.

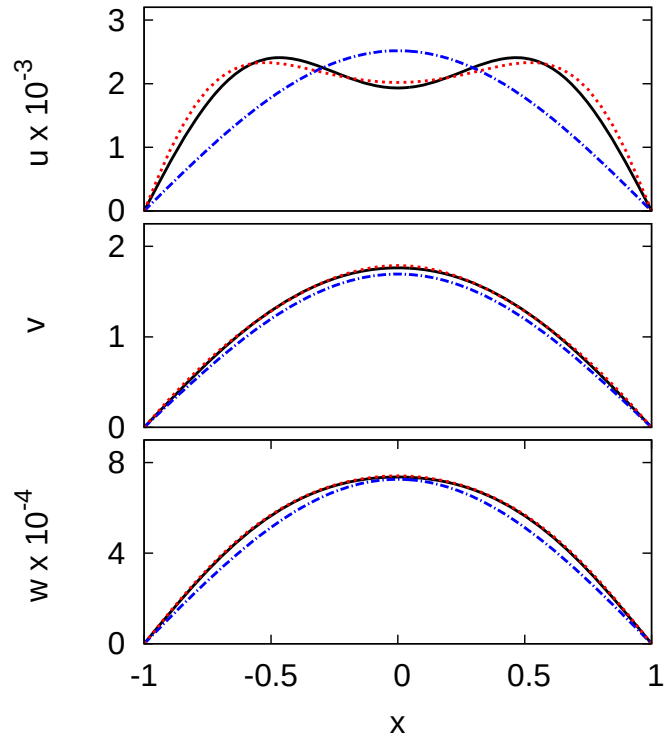

Fig. 2 (color online) The steady-state reactant concentrations u, v and w versus x, for the 1-D geometry. The parameter is $f = 8$. Shown are the one-term (dashed blue line) and two-term (black solid line) semi-analytical solutions and numerical (red dotted line) solutions of the governing PDEs.

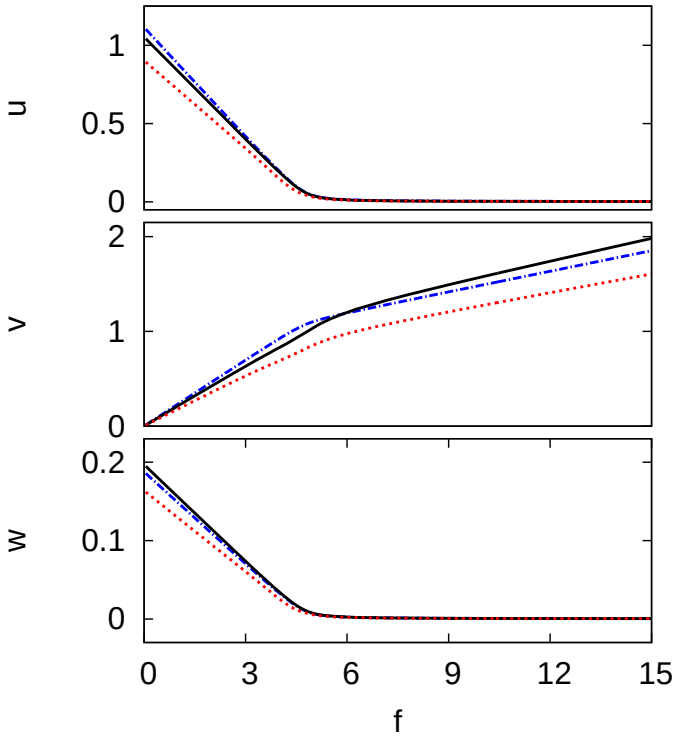

Fig. 3 (color online) The steady-state reactant concentrations u, v and w at $x = y = 0$ versus stoichiometric factor f, for the 2-D geometry. Shown are the one-term (dashed blue line) and two-term (black solid line) semi-analytical solutions and numerical (red dotted line) solutions of the governing PDEs (2).

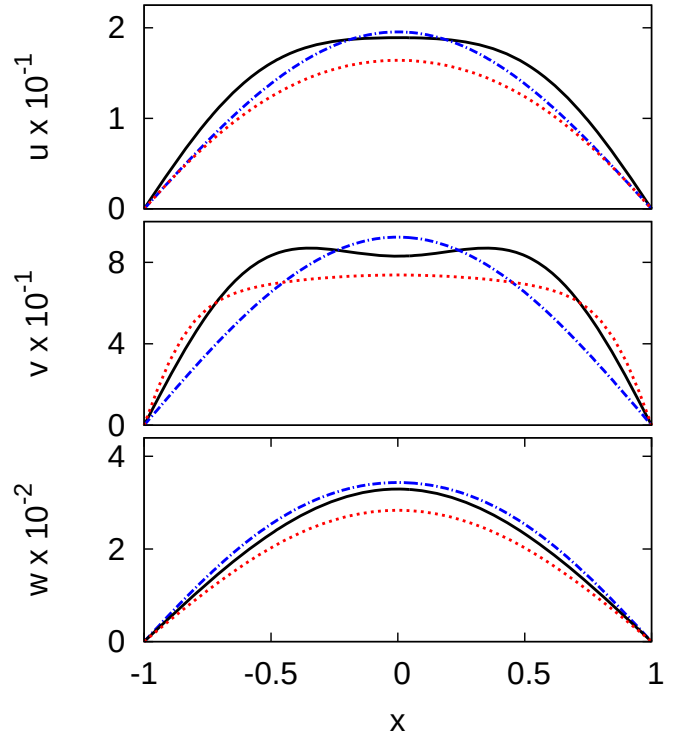

Fig. 4 (color online) The steady-state reactant concentrations u, v and w versus x, for the 2-D geometry. The parameter space is $f = 4$. Shown are the one-term (dashed blue line) and two-term (black solid line) semi-analytical solutions and numerical (red dotted line) solutions of the governing PDEs.

Figure 3 shows the steady-state reactant concentrations u, v and w versus the stoichiometric factor f, at the centre of the domain, $x = y = 0$, for the 2-D geometry. As in the 1-D case, the one and two-term semi-analytical and numerical solutions are shown. The curves in this case are qualitatively similar to figure 1 but the difference between the semi-analytical and numerical solutions is slightly larger, for large f values. There is a difference of 18% between the two-term semi-analytical and numerical solutions, up to $f = 15$. Semi-analytical solutions for a 2-D geometry generally have slightly larger errors than those in a 1-D geometry, see [28,29,8].

Figure 4 shows the steady-state reactant concentrations u, v and w versus x, for the 2-D case. Shown are the one-term and two-term semi-analytical solutions and numerical solutions of the governing PDE (2). The stoichiometric factor $f = 4$ and a slice for $y = 0$ are shown. The numerical solutions for v show a flatter concentration profile, which is more challenging to model with a series of trial functions. The two-term semi-analytical solution is superior to the one-term solution, but extra terms in the trial functions would be needed to further improve the comparison.

4 Stability analysis and Hopf bifurcations

In this section we discuss the stability of the BZ model in order to determine the parameter regions in which Hopf bifurcations points occur. Standard texts in bifurcation theory and dynamic systems describe the theory of Hopf bifurcations for delay systems, see [30,31]. Stability theory is well understood for systems of smooth ODEs but is less well developed for the non-smooth ODE system considered here, see [21] for a review of current theories. We use two approaches for the analysis of our semi-analytical non-smooth ODE system, which is comprised of eight sets of smooth ODEs. The first approach leads to the prediction of a band of parameter space, in which Hopf bifurcations for the full non-smooth system occur. The second approach is to consider the dominant eigenvalues of the system and the ideas of [21,22] who constructed a hybrid stability condition for a non-smooth system. This approach leads to a precise prediction of the region in which Hopf bifurcations occur, for the case of feedback with no delay.

4.1 Theoretical considerations

The 1-D model (6) and 2-D model (8) consist of ODEs for u_i, v_i and w_i. We write the modulus terms, of the form $|p|$, as $p\ \mathrm{sgn}(p)$ in the ODEs, and separately consider the stability of each smooth part of the system. As there are three different sign functions in the equations we get eight different sets of smooth ODEs. The smooth ODEs are expanded in a Taylor series about the steady-state solution. Let

$$u_i = u_{is} + \epsilon c e^{-\mu t}, \quad v_i = v_{is} + \epsilon g e^{-\mu t}, \quad w_i = w_{is} + \epsilon m e^{-\mu t}, \quad i = 1, 2 \ \ \epsilon \ll 1, \tag{9}$$

and substitute (9) into the systems (6) and (8), and then linearize around the steady state. The eigenvalues of the Jacobian matrix describes the growth of small perturbations in the system. This gives the characteristic equation $F(\mu) = m_1 + i m_2 = 0$ for the decay rate $\mu = w_1 + i w_2$. Hopf bifurcation points may 'occur at points where μ is purely imaginary. Here, the Hopf bifurcation points for the 1-D and 2-D cases are found by solving the system of equations

$$f_i = 0, \quad i = 1, 2, \ldots 6 \quad \text{and} \quad w_1 = m_1 = m_2 = 0, \tag{10}$$

where the f_i are the steady-state versions of the 1-D (6) and 2-D (8) models. For our system, this gives eight different regions in which Hopf bifurcations occur. Combining these results gives three regions: a region in which all sets of smooth ODEs of the system are stable; a region in which all smooth parts are unstable; and an intermediate region in which some smooth parts are stable and some are unstable. Hopf bifurcations for the full non-smooth ODE system occur in this intermediate region of the parameter space.

To help resolve the exact parameter space in which Hopf bifurcations occur the system considered in [21] provides some useful insights. They considered a linear system

$$\dot{\mathbf{x}} = \begin{cases} A^{-}\mathbf{x} & \text{if} \quad \mathbf{c}^T\mathbf{x} \leq 0, \\ A^{+}\mathbf{x} & \text{if} \quad \mathbf{c}^T\mathbf{x} \geq 0, \end{cases} \tag{11}$$

where the eigenvalues of $A^{\pm}$, $\lambda = \varsigma^{\pm} \pm i\omega^{\pm}$, $(\omega^{\pm} > 0)$, are complex, the steady state solution $\mathbf{x} = 0$ and $A^{\pm} \in R^{2\times 2}$, $\mathbf{c} = R^2$. Then the discontinuous system (11) is stable if $S < 0$ where

$$S = \frac{\varsigma^{+}}{\omega^{+}} + \frac{\varsigma^{-}}{\omega^{-}}. \tag{12}$$

An insight into this hybrid stability condition can be seen by considering the solutions

$$\mathbf{x} = \mathbf{d}e^{\varsigma^{\pm}t}\cos(\omega^{\pm}t), \tag{13}$$

of the two ODEs $\dot{\mathbf{x}} = A^{\pm}\mathbf{x}$. The solution stays in its portion of the phase plane space for time $t = \frac{\pi}{\omega^{\pm}}$, before the components of $\mathbf{x}$ change sign. Hence, the growth or decay during this time is $\frac{\varsigma^{\pm}\pi}{\omega^{\pm}}$, which leads to the hybrid stability condition $S < 0$.

For our system without delay, the one-term model consists of three ODEs and the two-term model consists of six ODEs. In the parameter region where the Hopf bifurcation occurs the long time behaviour is dominated by a complex conjugate pair of eigenvalues. The other eigenvalues have real parts that are more negative so can be ignored as they only affect the dynamics of the system at short times. Hence the dynamics of each smooth part of our system without delay is governed by a complex conjugate pair of eigenvalues, as in the linear system (11).

We now examine the perturbation (13) in more detail. If the components of the initial perturbation $\mathbf{d}$ are all positive (termed the *ppp* case), then the evolution of the perturbation (13) can only switch the system between the *ppp* and *nnn* (all negative components) cases. Hence in this case the perturbation to the non-smooth system will be stable if the dominant eigenvalues for the smooth ODE systems *nnn* and *ppp* satisfy $S < 0$. There are three other pairs of ODE systems (the *npn* and *pnp*, *ppn* and *nnp*, *pnn* and *npp* cases) for which similar switching can occur, so for each pair, the eigenvalues must also satisfy $S < 0$. The neutrally stable points are given by $S = 0$ for each pair of eigenvalues and points in the (f, k) plane which satisfy $S = 0$ are found using a bisection method.

However, for the case with delay the dynamics is no longer dominated by a single set of complex conjugate eigenvalues and a precise analytical description of the parameter space is not available. The reason for this is that the eigenvalue equation is not a cubic equation but a transcendental equation with an infinite number of solutions.

4.2 Hopf bifurcation regions and limit cycles for the 1-D geometry

In this section, the Hopf bifurcation parameter regions are obtained for 1-D geometry in two cases: feedback with no delay and feedback with delay. In each case, the Hopf bifurcation curves of the eight different smooth systems are found and curves plotted which divide the parameter space into three regions: one where no Hopf points occur; one where all the smooth systems predict Hopf points; and one region that has mixed stability. For the case with no delay precise semi-analytical estimates of the Hopf bifurcation parameter region are also obtained.

Figure 5 represents the region of Hopf bifurcations in the $f - k$ plane for the 1-D geometry with no delay. The parameters are $H = 0.1$ and $\tau = 0$. Figure 5(a) shows the two-term semi-analytical and numerical solutions. The semi-analytical predictions are of the stability of the sets of smooth ODEs, which divides the parameter space into three regions: one in which all smooth ODEs are stable, one in which they are all unstable; and one of mixed stability. The numerical Hopf bifurcation points lie inside the band of mixed stability. The Hopf bifurcation curves corresponding to the eight sets of smooth ODE systems do not intersect each other so the curves, which separate the parameter space into the three regions are smooth. Figure 5(b) shows the numerical Hopf

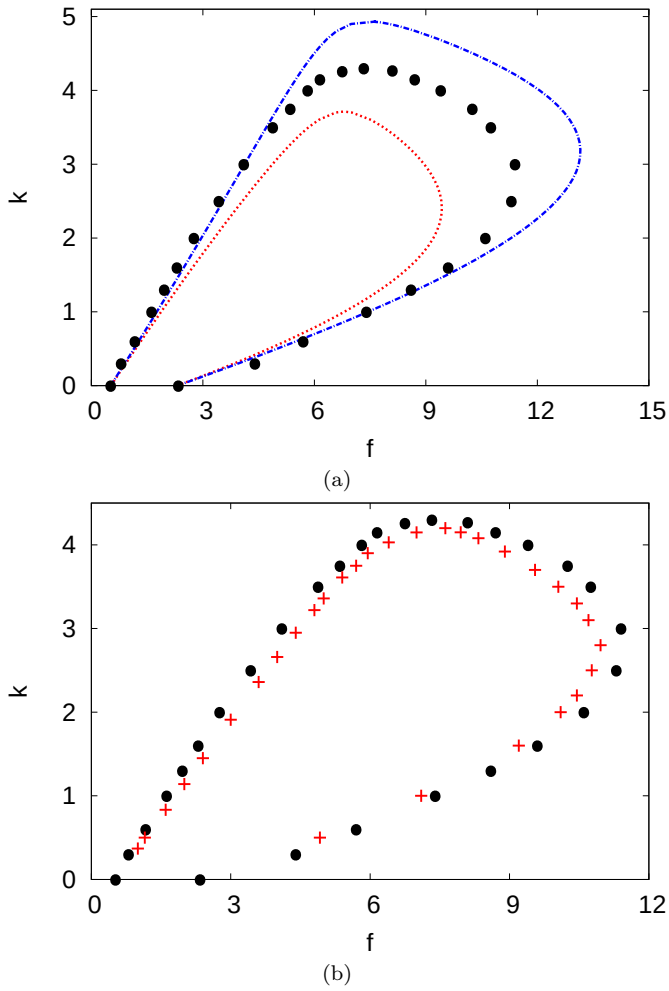

Fig. 5 (color online) The regions of the f-k plane in which Hopf bifurcations can occur for the 1-D geometry. The parameter values are $H = 0.1$ and $\tau = 0$. Shown in (a) are: the two-term semi-analytical (blue and red line) and numerical solutions (black dots), Shown in (b) are: numerical points of Hopf bifurcation for PDEs (black dots) and the theoretical prediction of $S = 0$ (red crosses).

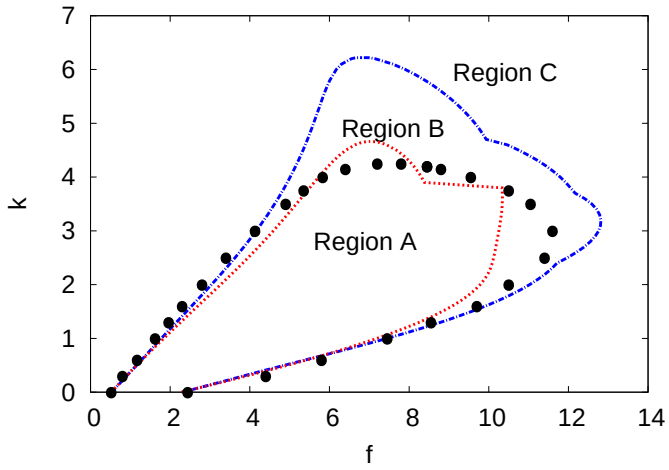

Fig. 6 (color online) The regions of the f-k plane in which Hopf bifurcations can occur for the 1-D geometry. Shown are the two-term semi-analytical (blue and red line) and numerical (black dots) solutions at parameter values $H = 0.1$ and $\tau = 1$.

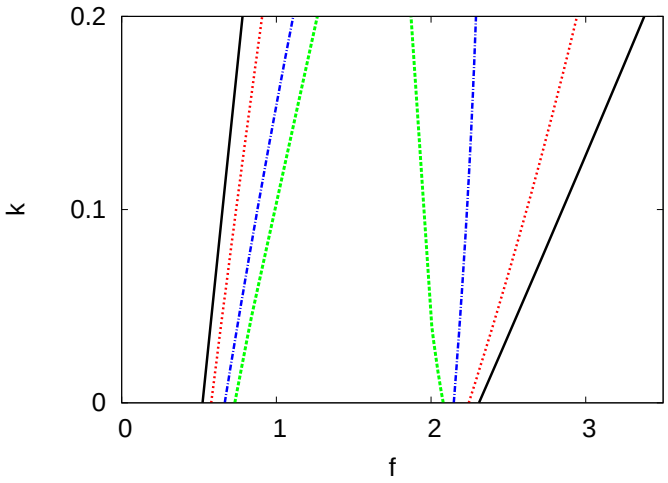

(a)- Feedback no delay ($\tau = 0$)

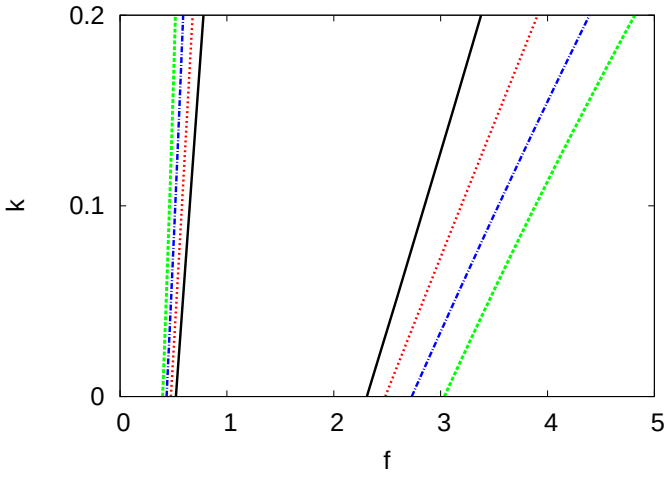

(b)- Feedback delay ($\tau = 1$)

Fig. 7 (color online) The regions of the f-k plane in which Hopf bifurcations can occur, for different values of H and small values of k. Shown are two-term semi-analytical solutions in the 1-D geometry for four different values of H: $H = 0$ (black solid line), $H = 1$ (red dotted line), $H = 2$ (dashed blue line) and $H = 4$ (green dotted line).

bifurcation points and the theoretical predictions of $S = 0$, from the two-term model. The neutral stability predictions, for each pair of ODEs, are the same, to graphical accuracy hence only one set of crosses are plotted on the figure. It can be seen that the theoretical estimates are very accurate with an error of less than 5% for all choices of f. It is also worth noting that $f \in [0, 4]$ for real chemical systems which corresponds to the lhs of the figures. For smaller f the inner and outer stability regions lie close together, except for some variations at large k.

Figure 6 represents the region of Hopf bifurcations in the $f - k$ plane for the 1-D geometry with delay feedback control. The parameters are $\tau = 1$ and $H = 0.1$. Shown are the two-term semi-analytical and numerical solutions. Again the numerical Hopf bifurcation points occur in the theoretical band of mixed stability. In the case with delay the smooth ODE Hopf bifurcation curves do intersect so the composite curves shown in Figure 6 are not smooth, unlike those in figure 5 for the no delay case. The stability formula (12) does not generalise to our system with delay and a precise estimate of the Hopf bifurcation region is not available. However for smaller values of the diffusion coefficient and the stoichiometric factor, $k \lesssim 2$ and $f \lesssim 4$ (which corresponds to chemically realistic values), the intermediate region of mixed stability is small and hence precise estimates of the region in which Hopf bifurcations occur, are available. For example, on the lhs of figure 6, at $k = 1$, the transition from region C to region A occurs for $f = 1.65$ and 1.70 for

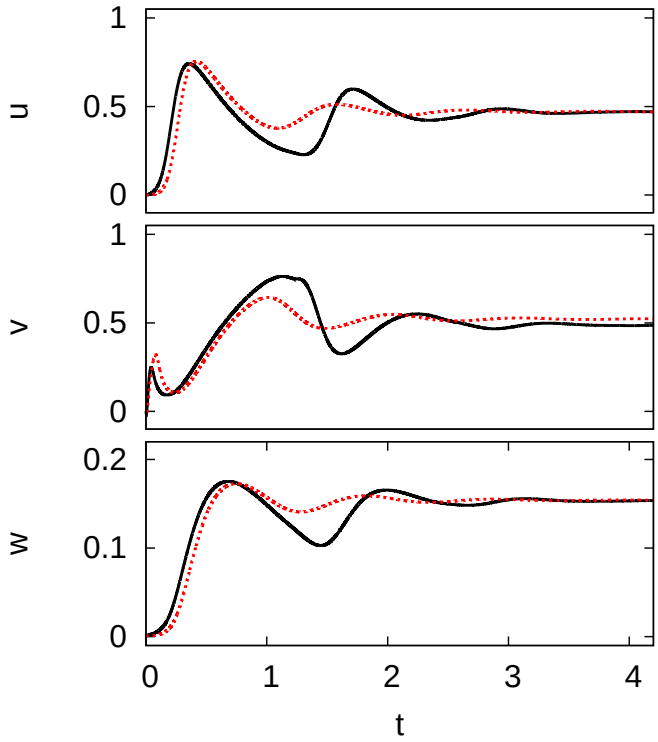

Fig. 8 (color online) The reactant concentrations u, v and w at $x = 0$ versus t for the 1-D geometry. The two-term semi-analytical solution (black solid line) and numerical solution (red dotted line) are shown. The parameters are $\tau = 1, H = 0.1$, $u_a = v_a = w_a = 0.1$, $k = 1$ and $f = 1.6$.

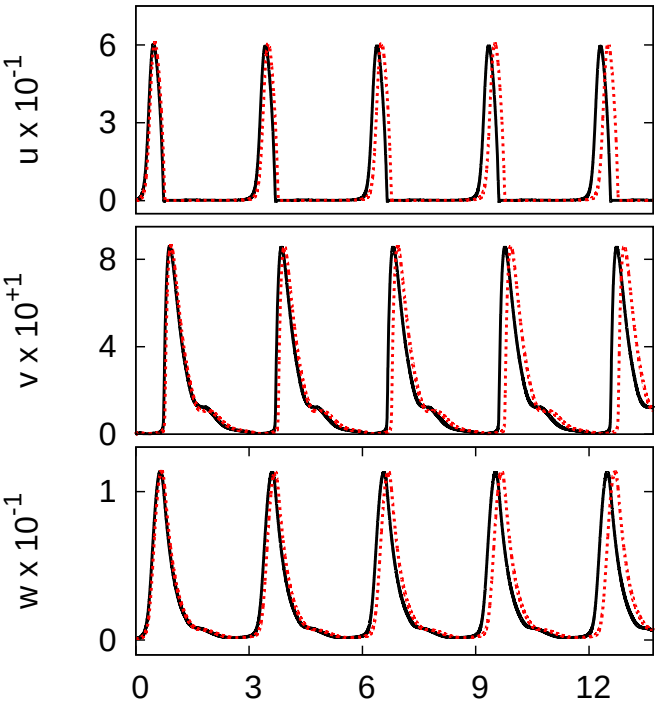

Fig. 9 (color online) The reactant concentrations u, v and w at $x = 0$ versus t for the 1-D geometry. The two-term semi-analytical solution (black solid line) and numerical solution (red dotted line) are shown. The parameters are $\tau = 1, H = 0.1$, $u_a = v_a = w_a = 0.1$, $k = 1$ and $f = 3$.

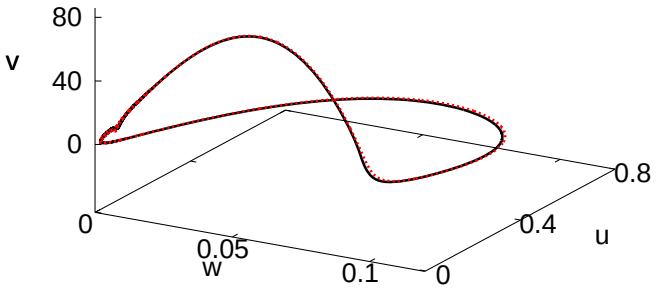

Fig. 10 (color online) The limit cycle when $f = 3, H = 0.1, k = 1$ and $\tau = 1$. The two-term (black solid line) semi-analytical and numerical solutions (red dotted line) are shown.

the numerical, and two-term semi-analytical solutions respectively. The two predictions are close, with only a 3% difference.

Figure 7 represents the Hopf bifurcation region in the $f - k$ plane, for the 1-D geometry, for small values of the diffusion coefficient. Shown is the two-term semi-analytical solution for $H = 0, 1, 2$ and 4. (a) is the no delay $\tau = 0$ case and (b) is for $\tau = 1$. For small values of the diffusion coefficient the stability predictions from the eight smooth systems are the same to graphical accuracy, so there is no band of mixed stability and a precise Hopf prediction is obtained. We can see that appropriately chosen values of H can stabilize or destabilize regions of parameter space. For figure 7(a), the case with no delay, we can see that as the feedback parameter H increases, the region of instability is decreasing. Figure 7(b) shows that as H increases, the region of instability increases. The effect of increasing H is stabilizing for small τ and destabilizing for large τ; the critical value of τ at which the behaviour changes is $\tau \approx 0.5$.

Figures 8 and 9 show the reactant concentrations u, v and w at $x = 0$, versus t for the 1-D geometry. The parameters are $u_a = v_a = w_a = 0.1$, $k = 1$, $H = 0.1$ and $\tau = 1$, with $f = 1.6$ (in region C of figure 6) for figure 8 and $f = 3$ (in region A of figure 6) for figure 9. The two-term semi-analytical and numerical solutions are shown. For figure 8 $f = 1.6$ and the solution evolves to a steady state, with $u_s \simeq 0.47$, $v_s \simeq 0.49$ and $w_s \simeq 0.15$ as the time becomes large, after some initial relaxation oscillations. The comparisons between the two-term semi-analytical and numerical solutions is excellent with only a maximum 1% error at the steady state. For figure 9 $f = 3$ and a periodic solution occurs. It can be seen that the maximum concentration of v is two orders of magnitude greater than that of u and w. This example represents a challenging test case for the semi-analytical solution method but the results prove to be highly accurate. The numerical amplitudes of the limit cycle for the reactant concentrations u, v and w are $0.60, 85.9$ and 0.11, respectively. These values are very close to the two-term semi-analytical results of $0.60, 85.6$ and 0.11, respectively. The errors in the two-term semi-analytical values are less than 0.5%.

Figure 10 is a view of the 3-D phase space. The two-term semi-analytical and the numerical solutions in the 1-D geometry are shown. The parameters are $f = 3, k = 1$ and $\tau = 1$. The numerical period of the limit cycle for the reactants is 3.00, while the two-term semi-analytical period of the limit cycle is 2.97, a difference of only 1%. The two-term semi-analytical approximation is fairly close to the numerical solution over the whole parameter space and the semi-analytical limit cycle has many quantitative similarities to the numerical solution.

4.3 Hopf bifurcation regions and limit cycles for the 2-D geometry

Figure 11 represents the region of Hopf bifurcations in the $f - k$ plane for the 2-D geometry with no delay. The parameters are $H = 0.1$ and $\tau = 0$. Figure 11(a) shows the two-term semi-analytical and numerical solutions. The stability of the smooth ODE systems give a band of parameter space in which Hopf bifurcations occur. As in the 1-D, there are three regions and the numerical Hopf bifurcations occur in the band region which has mixed stability. As for the 1-D case the composite

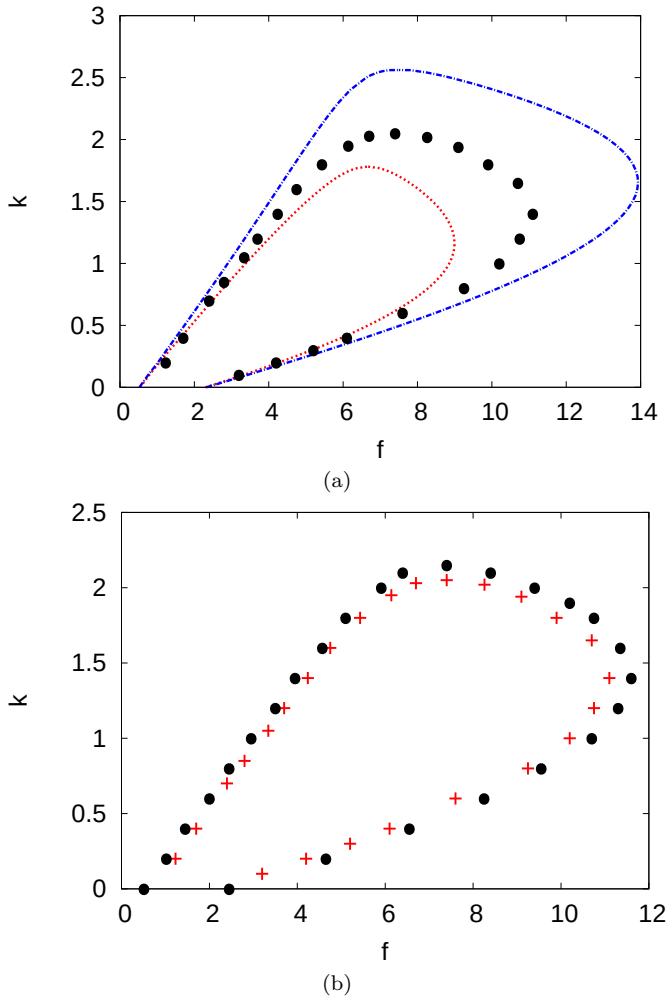

Fig. 11 (color online) The region of the f-k plane in which Hopf bifurcations can occur for the 2-D geometry. The parameters are $H = 0.1$ and $\tau = 0$. Shown in (a) are the two-term semi-analytical (blue and red line) and numerical solutions (black dots), Shown in (b) are the numerical points of Hopf bifurcation (black dots) and the theoretical prediction $S = 0$ (red crosses).

curves in figure 11(a) are smooth. Figure 11(b) shows numerical Hopf bifurcations and theoretical predictions of $S = 0$ for the four pairs of ODE systems from the two-term model (which are all the same to graphical accuracy). Also, as for the case of 1-D geometry the prediction is excellent, with an error of less than 9% between them at all choices of f. As for the 1-D geometry the inner and outer stability regions lie close together for small f (which corresponds to chemically realistic values), except for some variations at large k.

Figure 12 represents the region of Hopf bifurcations in the $f - k$ plane, for the 2-D geometry with delay. The parameters are $\tau = 1$ and $H = 0.1$. Shown are the two-term semi-analytical and numerical solutions. As in the 1-D geometry, this figure shows three different regions: one stable, one unstable, and one of mixed stability. It can be seen that the numerical Hopf bifurcation points occur in the region of mixed stability and are close to the border with the unstable region. Hence nearly all of smooth ODE systems need to be unstable for the full non-smooth system to destabilize. As for the 1-D geometry case the intermediate region is small for smaller values of the diffusion coefficient $k \lesssim 1$. One the left hand side of the figure at $k = 1$, for the transition from region C to region A, the Hopf points are given by $f = 2.90$ and 3.12, for the numerical and two-term semi-analytical solutions respectively, which is a 7% difference.

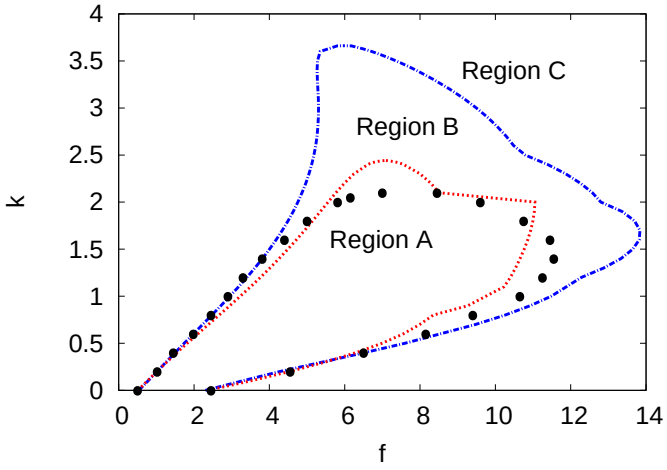

Fig. 12 (color online) The region of the f-k plane in which Hopf bifurcations can occur for the 2-D geometry. Shown are the two-term semi-analytical (blue and red line) and numerical (black dotted) solutions at parameters $H = 0.1$ and $\tau = 1$.

Figure 13 represents the Hopf bifurcation region in the $f - k$ plane for the 2-D geometry, for small values of the diffusion coefficient. Shown is the two-term semi-analytical solution for $H = 0$, 0.5, and 1. (a) is the no delay $\tau = 0$ case and (b) is for $\tau = 1$. As in the 1-D case, it can see that appropriately chosen values of H can stabilize or destabilize regions of parameter space. For figure 13(a) shows the case with feedback with no delay and we can seen that as the feedback parameter H increases, the region of instability decreases. The figure 13(b) shows the case with delay feedback at $\tau = 1$. In this case as H increases the region of instability grows. As in 1-D, the effect of increasing H for small τ is stabilizing and destabilizing for large τ; the critical $\tau \approx 0.6$.

Figures 14 and 15 show the reactant concentrations u, v and w at $x = y = 0$ versus t for the 2-D geometry. The parameters are $u_a = v_a = w_a = 0.1$ and $\tau = 1$ with $f = 2.7$ (from region C in figure 12) for figure 14 and $f = 3.5$ (from region A in figure 12) for figure 15. The two-term semi-analytical and numerical solutions are shown. For figure 14 $f = 2.7$ and the solution evolves to a steady state, with $u_s \simeq 0.47$, $v_s \simeq 0.57$ and $w_s \simeq 0.09$ as the time becomes large. The comparison between the numerical and the two-term semi-analytical solutions shows a 18% difference in the steady state. For figure 15 $f = 3.5$, so periodic solutions occur. The numerical amplitudes of the limit cycle for u, v and w are $0.50, 34.4$ and 0.07 respectively. These values are fairly close to the two-term values of $0.58, 41.9$ and 0.08 respectively. As in the 1-D case, the two-term semi-analytical method is again accurate, with errors of less than 18%.

Figure 16 is a view of the 3-D phase space. The two-term semi-analytical and the numerical solutions for the PDEs in the 2-D geometry are shown. The parameter choices are $f = 3.5, k = 1$ and $\tau = 1$. The numerical and two-term semi-analytical periods of the limit cycle of the reactant at concentrations u, v and w are 1.55 and 1.49 respectively. The errors in the two-term semi-analytical values are less than 4%. As for the 1-D case, the semi-analytical solution for the ODEs model is close to the numerical solution of the PDEs, in this 3-D parameter space.

5 Conclusion

This paper has presented semi-analytical solutions for the BZ model in a reaction-diffusion cell with feedback control for both the 1-D and 2-D geometries. The Galerkin method was used to approximate the governing delay PDEs by a system of delay ODEs. A key feature of the problem is the non-smooth nature of the feedback control and the challenges this presents for analytical investigation. For the no delay case the consideration of the dominant eigenvalues together with a hybrid stability condition allows an accurate semi-analytical prediction of the Hopf bifurcation region to be found. For cases with feedback delay a band of parameter space is found in which the

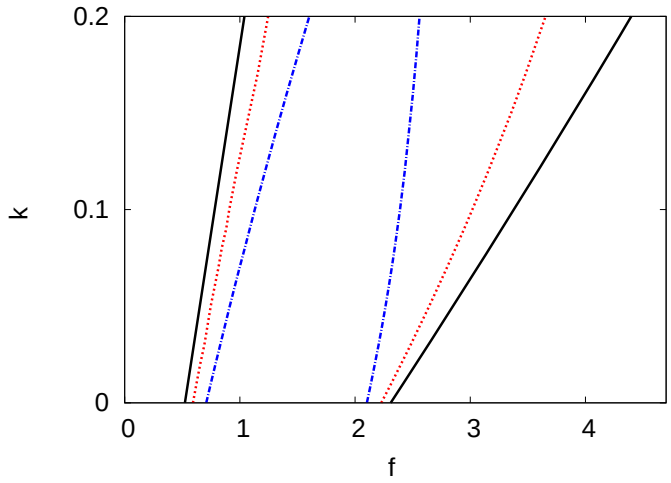

(a)- Feedback no delay ($\tau = 0$)

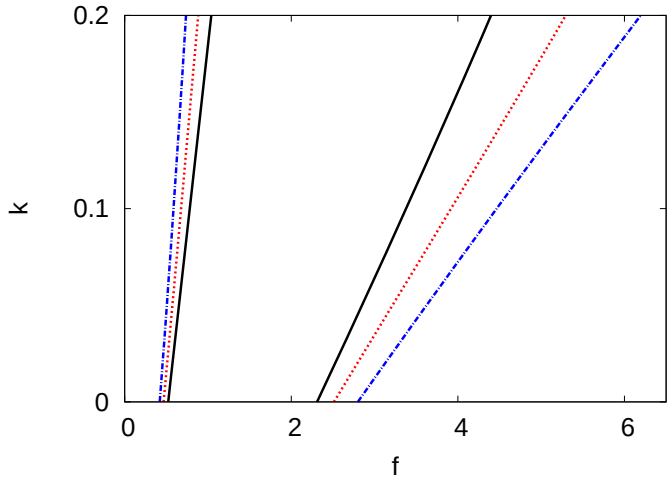

(b)- Feedback delay ($\tau = 1$)

Fig. 13 (color online) The region of the f-k plane in which Hopf bifurcations can occur, for different values of H and small values of k. Shown are two-term semi-analytical solutions in the 2-D geometry for three different examples of H: $H = 0$ (black solid line), $H = 0.5$ (red dotted line) and $H = 1$ (dashed blue line).

Hopf points occur. The effect of feedback is stabilizing for small delay and destabilizing for large delay. Examples of stable and unstable limit cycles were obtained with a good comparison between semi-analytical and numerical solutions. This work illustrates the usefulness of the Galerkin averaging technique, for reaction diffusion equations and also contributes to the understanding of stability for non-smooth systems with multiple delay terms.

Future work could involve extending the method to other classes of oscillatory chemical systems, for which the model equations are much more complex than the Oregonator model. Also the results illustrate a range of interesting behaviours that can occur in the reaction-diffusion cell with boundary feedback control. Hopefully this study will motivate new experimental work using this type of feedback scenario.

Acknowledgement: The authors would like to thank an anonymous referee for their useful comments

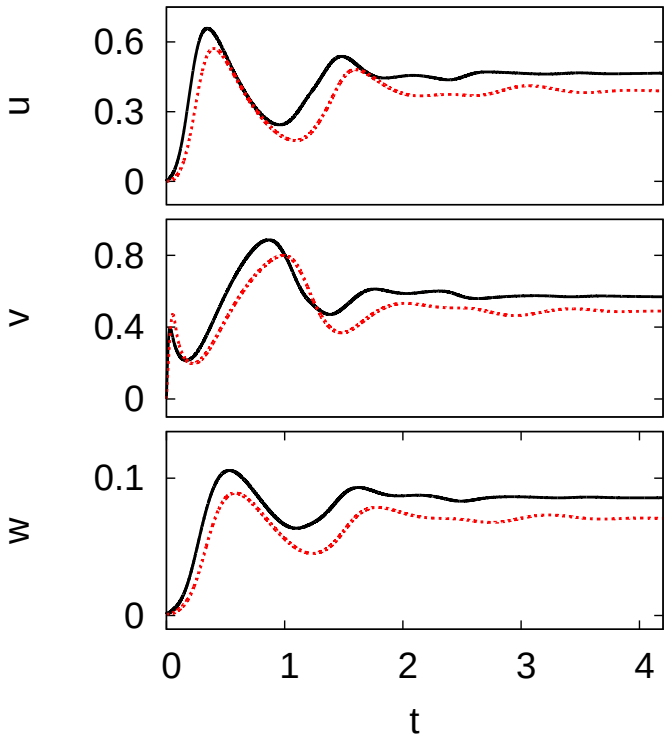

Fig. 14 (color online) The reactant concentrations u, v and w at $x = y = 0$ versus t for the 2-D geometry. The two-term semi-analytical solution (black solid line) and numerical solution (red dotted line) are shown. The parameters are $\tau = 1, H = 0.1$, $u_a = v_a = w_a = 0.1$, $k = 1$ and $f = 2.7$.

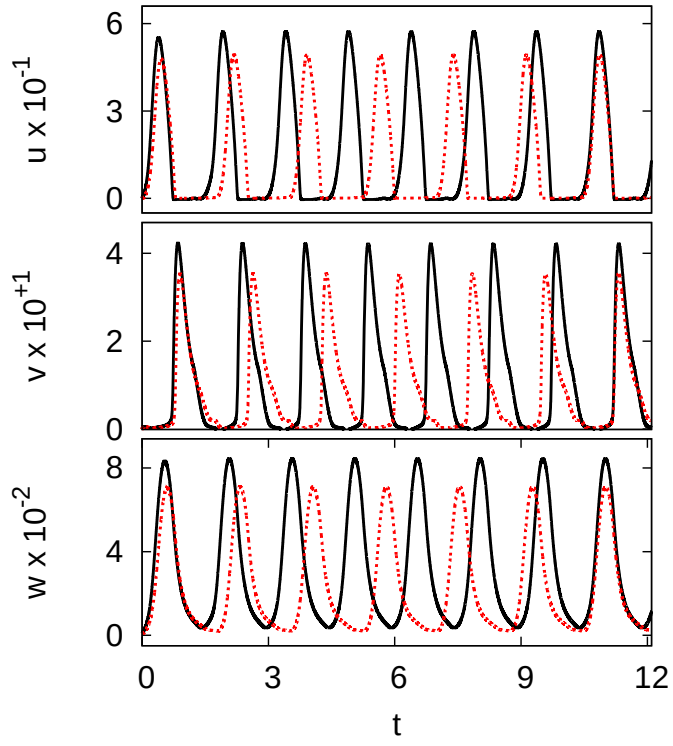

Fig. 15 (color online) The reactant concentrations u, v and w at $x = y = 0$ versus t for the 2-D geometry. The two-term semi-analytical solution (black solid line) and numerical solution (red dotted line) are shown. The parameters are $\tau = 1, H = 0.1$, $u_a = v_a = w_a = 0.1$, $k = 1$ and $f = 3.5$.

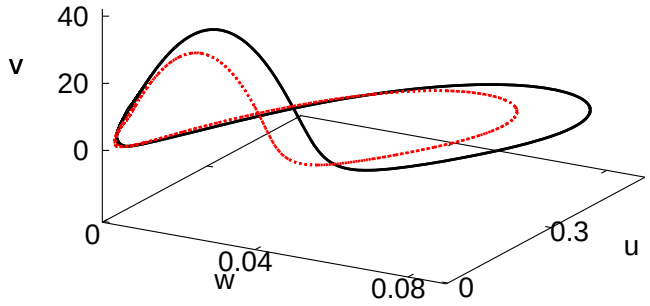

Fig. 16 (color online) The limit cycle when $f = 3.5, H = 0.1, k = 1$ and $\tau = 1$. The two-term (black solid line) semi-analytical and numerical solutions (red dotted line) are shown.

Appendix: Expressions for the semi-analytical ODEs.

This appendix presents relevant expression for for the semi-analytical models. The M_i for the 1-D model (6) are

$$
\begin{aligned}
M_1 &= \frac{2H}{\epsilon}u_d v_d + \frac{2H}{\epsilon}u_d^2 - \frac{20H}{3\epsilon\pi}u_d v_d - \frac{1}{\epsilon}u_d + \frac{16u_1}{3\epsilon\pi}u_d + \frac{16u_2}{15\epsilon\pi}u_d + \frac{8u_1}{3\epsilon\pi}v_d + \frac{k\pi^2}{4}u_d - \frac{q}{\epsilon}v_d \\
&+ \frac{8v_2}{15\epsilon\pi}u_d - \frac{v_1}{\epsilon}u_d - \frac{20H}{3\epsilon\pi}u_d^2 - \frac{2u_1}{\epsilon}u_d - \frac{u_1}{\epsilon}v_d, \\
M_2 &= \frac{2H}{\delta}u_d v_d + \frac{8u_1}{3\delta\pi}v_d - \frac{20H}{3\delta\pi}u_d v_d + \frac{8v_2}{15\delta\pi}u_d - \frac{u_1}{\delta}v_d - \frac{4q}{\delta\pi}v_d + \frac{8v_1}{3\delta\pi}u_d + \frac{k\pi^2}{4}v_d - \frac{v_1}{\delta}u_d \\
&- \frac{f}{\delta}w_d + \frac{8u_2}{15\delta\pi}v_d + \frac{4f}{\delta\pi}w_d + \frac{q}{\delta}v_d, \\
M_3 &= \frac{4}{\pi}u_d - u_d + w_d + \frac{k\pi^2}{4}w_d - \frac{4}{\pi}w_d, \\
M_4 &= \frac{8v_1}{15\epsilon\pi}u_d + \frac{8u_1}{15\epsilon\pi}v_d + \frac{144}{35\epsilon\pi}u_d - \frac{4}{3\epsilon\pi}u_d + \frac{4H}{5\epsilon\pi}u_d v_d + \frac{4H}{5\epsilon\pi}u_d^2 + \frac{72u_2}{35\epsilon\pi}v_d - \frac{2u_2}{\epsilon}u_d + \frac{16u_1}{15\epsilon\pi}u_d \\
&+ \frac{72v_2}{35\epsilon\pi}u_d - \frac{v_2}{\epsilon}u_d - \frac{u_2}{\epsilon}v_d + \frac{4q}{3\epsilon\pi}v_d, \\
M_5 &= \frac{4q}{3\delta\pi}v_d - \frac{4f}{3\delta\pi}w_d + \frac{72v_2}{35\delta\pi}u_d + \frac{72u_2}{35\delta\pi}v_d + \frac{4}{5\delta\pi}u_d v_d + \frac{8u_1}{15\delta\pi}v_d + \frac{8v_1}{15\delta\pi}u_d - \frac{u_2}{\delta}v_d - \frac{v_2}{\delta}u_d, \\
M_6 &= \frac{4}{3\pi}w_d - \frac{4}{3\pi}u_d.
\end{aligned}
$$

The N_i for the 2-D model (8) are

$$
\begin{aligned}
N_1 &= \frac{64u_1}{9\epsilon\pi^2}v_d + \frac{128v_2}{45\epsilon\pi^2}u_d + \frac{16q}{\epsilon\pi^2}v_d^2 + \frac{128u_2}{45\epsilon\pi^2}u_d + \frac{2H}{\epsilon}u_d^2 + \frac{64v_1}{9\epsilon\pi^2}u_d - \frac{q}{\epsilon}v_d + \frac{k\pi^2}{2}u_d + \frac{256u_2}{45\epsilon\pi^2}u_d \\
&+ \frac{16}{\epsilon\pi^2}u_d - \frac{208H}{9\epsilon\pi^2}u_d v_d + \frac{2H}{\epsilon}u_d v_d - \frac{208H}{9\epsilon\pi^2}u_d^2 - \frac{2u_1}{\epsilon}u_d + \frac{128u_1}{9\epsilon\pi^2}u_d - \frac{v_1}{\epsilon}u_d - \frac{u_1}{\epsilon}v_d - \frac{1}{\epsilon}u_d, \\
N_2 &= -\frac{208H}{9\delta\pi^2}v_d u_d + \frac{2H}{\delta}v_d u_d + \frac{64v_1}{9\delta\pi^2}u_d + \frac{k\pi^2}{2}v_d + \frac{128v_2}{45\delta\pi^2}u_d + \frac{64u_1}{9\delta\pi^2}v_d - \frac{v_1}{\delta}u_d - \frac{16q}{\delta\pi^2}v_d + \frac{q}{\delta\pi^2}v_d \\
&+ \frac{16f}{\delta\pi^2}w_d - \frac{f}{\delta}w_d + \frac{128u_2}{45\delta\pi^2}v_d - \frac{u_1}{\delta}v_d, \\
N_3 &= \frac{k\pi^2}{2}w_d - \frac{16}{\pi^2}w_d + \frac{16}{\pi^2}u_d + w_d - u_d, \\
N_4 &= -\frac{16q}{3\epsilon\pi^2}v_d - \frac{2u_2}{\epsilon}u_d + \frac{9088u_2}{1575\epsilon\pi^2}v_d - \frac{v_2}{\epsilon}u_d + \frac{176H}{45\epsilon\pi^2}u_d^2 + \frac{176H}{45\epsilon\pi^2}u_d v_d + \frac{64v_1}{45\epsilon\pi^2}u_d + \frac{9088v_2}{1575\epsilon\pi^2}u_d \\
&+ \frac{64u_1}{45\epsilon\pi^2}v_d + \frac{18176u_2}{1575\epsilon\pi^2}u_d + \frac{128u_1}{45\epsilon\pi^2}u_d - \frac{u_2}{\epsilon}v_d - \frac{16}{3\epsilon\pi^2}u_d, \\
N_5 &= \frac{16q}{3\delta\pi^2}v_d - \frac{v_2}{\delta}u_d + \frac{64v_1}{45\delta\pi^2}u_d + \frac{9088u_2}{1575\delta\pi^2}v_d + \frac{176H}{45\delta\pi^2}u_d v_d + \frac{64u_1}{45\delta\pi^2}v_d - \frac{16f}{3\delta\pi^2}w_d + \frac{9088v_2}{1575\delta\pi^2}u_d - \frac{u_2}{\delta}v_d, \\
N_6 &= \frac{16}{3\pi^2}w_d - \frac{16}{3\pi^2}u_d.
\end{aligned}
$$

The delay terms are defined as

$$
\begin{aligned}
&u_d = |u_{1s} + u_{2s} - u_1(t-\tau) - u_2(t-\tau)|, \quad v_d = |v_{1s} + v_{2s} - v_1(t-\tau) - v_2(t-\tau)|, \\
&w_d = |w_{1s} + w_{2s} - w_1(t-\tau) - w_2(t-\tau)|.
\end{aligned}
$$

References

1. Corbel, J.M.L., Van Lingen, J.N.J., Zevenbergen, J.F., Gijzeman, O.L.J., Meijerink, A. Strobes: pyrotechnic compositions that show a curious oscillatory combustion. Angew. Chem. Int. Ed. **52** 290–303 (2013)
2. Belousov, B.P. An oscillating reaction and its mechanism. Sborn. Referat. Radiat. Med., (Medgiz, Moscow), 145 (1959)
3. Sagues, F., Epstein, I.R. Nonlinear chemical dynamics. Dalton. Trans. **7** 1201–1217 (2003)
4. Field, R.J., Körös, E., Noyes, R. Oscillations in chemical systems. II. thorough analysis of temporal oscillation in the Bromate-Cerium-Malonic Acid system. J. Am. Chem. Soc. **94** 8649–8664 (1972)
5. Field, R.J., Noyes, R.M. Oscillations in chemical systems. IV. limit cycle behavior in a model of a real chemical reaction. J. Chem. Phys. **60** 1877– 1884 (1974)
6. Tyson, J.J. The Belousov-Zhabotinskii Reaction. Springer-Verlag, New York (1976)
7. Tyson, J.J. Oscillations, Bistability and echo waves in models of the Belousov-Zhabotinskii reaction. Ann. New York Acad. Sci. **316** 279–295 (1979)
8. Marchant, T.R. Cubic autocatalytic reaction-diffusion equations: semi-analytical solutions. Proc. R. Soc. Lond. **A458** 873–888 (2002)
9. Marchant, T.R. Cubic autocatalysis with Michaelis-Menten kinetics: semi-analytical solutions for the reaction-diffusion cell. Chem. Engng. Sci. **59** 3433–3440 (2004)
10. Forbes, L. Stationary patterns of chemical concentration in the Belousov-Zhabotinskii reaction. Physica D **43** 140–152 (1990)
11. Forbes, L. On stability and uniqueness of stationary one-dimensional patterns in the Belousov-Zhabotinsky reaction. Physica D **50** 42–58 (1991)
12. Noszticzius, Z., Horstemke, W., McCromick, W.D., Swinney, H.L., Tam, W., Sustained chemical waves in an annular gel reactor: a chemical pinwheel. Nature **329** 619–620 (1987)
13. Tam, W., Horstemke, W., Noszticzius, Z., Swinney, H.L. Sustained sprial waves in a continuously fed unstrirred chemical reactor. J. Chem. Phys. **88** 3395–3396 (1988)
14. Bagyan, S., Mair, T., Dulos, E., Boissonade, J., DeKepper, P., Muller, S. Glycolytic oscillations and waves in an open spatial reactor: Impact of feedback regulation of phosphofructokinase. Biophys. Chem. **116** 67–76 (2005)
15. Lavrova, A., Bagyan, S., Mair, T., Hauser, M., Schimansky-Geier, L. Modeling of glycolytic wave propagation in an open spatial reactor with inhomogeneous substrate flux. Biosystems **97** 127–133 (2005)
16. Sriram, K. Effects of positive electrical feedback in the oscillating Belousov-Zhabotinsky reaction: Experiments and simulations. Chaos Soliton Fract. **28** 1055–1066 (2006)
17. Zhu, R., Qian, L. Eliminating chaos in the Belousov-Zhabotinsky reaction by no-delay feedback and delayed feedback. Theor. Chem. Acc. **110** 85–91 (2003)
18. Györgyi, L., Field, R.J. A three-variable model of deterministic chaos in the Belousov-Zhabotinsky reaction. Nature **335** 808–810 (1992)
19. Lipták, G., Szederkényi, G., Hangos, K. M. Hamiltonian feedback design for mass action law chemical reaction networks. IFAC Papers Online **48-13** 158-163 (2015)
20. Vanag, V., Epstein, I.R. Design and control of patterns in reaction-diffusion systems. Chaos **18** 026107 (2008)
21. di Bernardo, M., Budd, C., Champneys, A.R., Kowalczyk, P. Piecewise-Smooth Dynamical Systems: Theory and Applications. London, Springer (2008)
22. Camlibel, M.K., Heemels, W., Schumacher, J.M. Stability and controllability of planar linear bimodal complementarity systems. In: Proceedings of the 42nd IEEE Conference on decision and control, Hawai, USA 1651–1656 (2003)
23. Csikja, R., Garay, B.M., Tóth, J. Chaos via two-valued interval maps in a piecewise affine model example for hysteresis. In: Proceedings of the 19th International Symposium on Mathematical Theory of Networks and Systems, Hungary 187-194 (2010)
24. Takada, H., Shimizu, Y., Miyao, M. The number of autocatalytic reactions in systems of oscillating reactions. Forma **18** 67–82 (2003)
25. Vanag, V., Zhabotinsky, A., Epstein, I. Pattern formation in the Belousov-Zhabotinsky reaction with photochemical global feedback. J. Phys. Chem. A **104** 11566–11577 (2000)
26. Jahne, W., Winfree, A.T. A survey of spiral wave behaviours in the Oregonator model. Int. J. Bifurc. Chaos **1** 445– (1991)
27. Ropp, D.L., Shadid, J.N. Stability of operator splitting methods for systems with indefinite operators: reaction-diffusion systems. J. Comput. Phys. **203** 449–466 (2005)
28. Alfifi, H.Y., Marchant, T.R., Nelson, M.I. Generalised diffusive delay logistic equations: semi-analytical solutions. Dynam. Cont. Dis. Ser. B **19** 579–596 (2012)
29. Alfifi, H.Y., Marchant, T.R., Nelson, M.I. Semi-analytical solutions for the 1- and 2-D diffusive Nicholson's blowflies equation. IMA J. Appl. Math. **79** 175-199 (2014)
30. Erneux, T. Applied Delay Differential Equations. Springer, New York (2009)
31. Hale, J. Theory of Functional Differential Equations. Springer Verlag, New York (1977)